RSC Advances

Accepted Manuscript

ROYAL SOCIETY OF CHEMISTRY

rsc.li/rsc-advances

Grafting modification of epoxidized natural rubber with poly (ethylene glycol) monomethylether carboxylic acid and ionic conductivity of graft polymer composite electrolytes

RanWang, HuaMei. Wentan Ren*, YongZhang
School of Chemistry and Chemical Engineering, Shanghai Jiao Tong University

Abstract

A novel comb-like polymer was synthesized via grafting epoxidized natural rubber (ENR) with polyethylene glycol (PEG) monomethylether carboxylic acid (mPEG-COOH), and the grafting reaction was studied by variable-temperature Fourier transform infrared (FTIR) spectroscopy. This comb-like polymer was characterized by attenuated total reflectance-FTIR (ATR-FTIR) spectroscopy and differential scanning calorimetry (DSC). The carboxyl groups of mPEG-COOH reacted with the epoxy groups of ENR to produce graft polymers. Composite polymer electrolyte (CPE) based on this comb-like polymer ENR-*g*-mPEG-COOH was prepared *via* introducing $LiClO_4$ into graft polymer matrix. The CPE was studied by X-ray diffraction analysis (XRD), DSC, equilibrium swelling method, and electrochemical workstation techniques. With increasing mPEG-COOH content, the ionic conductivity of the electrolyte significantly increased.

Keywords: grafting reaction; epoxidized natural rubber; mPEG-COOH; coordination crosslinking; ionic conductivity

Introduction

Polymer composites electrolytes (PEs) attracted abundant research in the past few decades.[1-4] Enjoying a high capacity to dissolve lithium salts and ionic conductivity above 70 °C, polyethylene oxide (PEO) is the most studied polymer electrolyte matrix [2, 5-7]. However, the conductivity of PEO is still limited by its inherent crystallization at room temperature [8, 9]. Researchers went off the beaten track and designed rubbers as polymer matrix. Elastomers, especially rubber, are notable for their excellent elasticity, low glass transition temperature (T_g) and soft elastomeric nature at room temperature [10]. Many modification methods based on elastomers, such as introducing grafting[11]

and crosslinking structure[12], adding inorganic fillers[1, 13, 14], have already successfully applied in obtaining new polymer electrolytes.

Epoxidized natural rubber (ENR), a modified form of natural rubber, has good potential to become a polymer host in CPE because of its distinctive characteristic such as low T_g, soft elastomeric characteristics at room temperature [15] and good electrode-electrolyte adhesion. The liquid ENR and poly(vinyl) chloride (PVC) blends are also used as a host for PEs.[4] In ENR-based polymer electrolytes, the highly flexible macromolecular chains and the polar epoxy groups of ENR provide excellent segmental motion, coordination sites for Li^+ transport and reactivity with other groups like carboxyl and amine groups[16, 17]. Furthermore, ENR also offers good contact between electrolytic layer and electrode for batteries [18].

mPEG-COOH is a carboxylated compound of polyethylene glycol mono methyl ether. The ether oxygen groups on the polyethylene glycol chain have coordination reactivity with the cation to make it dissolve, and have the best space coordination to form a homogeneous system. Therefore, polyethylene glycol is widely used in polymeric electrolytes. A new PEG-based PEs is developed for quasi-solid-state battery application.[19] However, a large amounts of liquid electrolytes is needed in this system, which might be evaporated at high temperature and thus would lower the conductivity.[20] Hence, in order to obtain more stable and highly ionic conductive polymer electrolytes, modifying polymer is necessary.

This paper mainly studied the graft modification between ENR 50 and mPEG-COOH, which could inhibit the crystallization for mPEG-COOH and improve the conductivity of CPE. The grafting reaction and the structure of graft polymer ENR-*g*-mPEG-COOH was investigated by heated infrared spectroscopy (FTIR), ATR-FTIR and DSC. By adding lithium salt $LiClO_4$, crosslinked polymer electrolyte ENR-*g*-mPEG-COOH /$LiClO_4$ was also prepared by the coordination effect. The CPE were characterized by DSC, XRD and the equilibrium swelling method. The effect of mPEG-COOH content on the ionic conductivity was also discussed.

2 Experimental

2.1 Materials

The ENR used was epoxidized natural rubber with 50% epoxidation and the trade name is ENR 50, produced by the Chinese Academy of Tropical Agricultural Sciences (CATAS, Hainan, China), and its structure was shown in Fig.1(a). mPEG-COOH (98.8%, M_w=2000) was purchased from YaRe Biological Technology Co. Ltd. (Shanghai, China), and its structure was shown in Fig.1(b).

All solvents including tetrahydrofuran (THF), *N,N*-dimethylformamid (DMF), methanol, toluene and methanol were supplied by Sinopharm Reagent Co. Ltd., China.

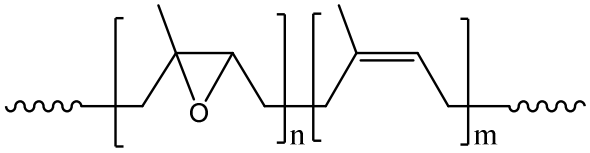

(a)

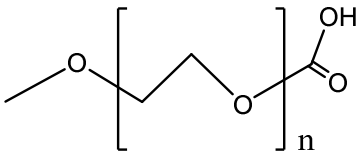

(b)

Fig.1 Structures of ENR 50 (a) and mPEG-COOH (b).

2.2 Sample preparation

ENR 50 was first dissolved in THF and then precipitated in methanol for purification. The precipitated ENR was washed with methanol for several times before vacuum dried at 40°C for 24 h. ENR 50 solutions in DMF (70 mL) containing 5, 10, 15, 20, 30, 40, 60 and 80 phr (per hundred rubber by weight) mPEG-COOH were stirred mechanically in oil bath at 140°C for 8h in nitrogen atmosphere and then rotary evaporation was used to remove the excess solvent. Then the product was vacuum dried at 80°C for 12 h. The samples were extracted with methanol for 24 h, and then the purified products were dried in a vacuum oven at 25°C for 3 days. Therefore, graft polymer ENR-*g*-mPEG-COOH was obtained as a CPE matrix.

The graft polymer ENR-*g*-mPEG-COOH was dissolved in THF (30 mL), then $LiClO_4$ (40 phr) was added and stirring for 3h. The solution was poured into Teflon mould, and the solvent was evaporated at room temperature. Further drying of the solutions was then conducted in a vacuum oven at 40°C for 24 h. Finally, the CPE films were successfully prepared.

2.3 Characterization and instruments

2.3.1 The process of the grafting reaction

In situ FTIR spectroscopy

FTIR spectra of ENR /mPEG-COOH mixture were recorded to study the process of the grafting reaction. ENR 50 and mPEG-COOH (100/80) dissolved in THF were dropped on KBr pellets and transferred to a temperature-controlled cell in an FTIR spectrometer (NEXUS 470). Testing temperature increased from 40 to 170°C at a heating rate of 5°C min^{-1}. FTIR spectra were recorded when the temperature increased by every 10 °C. Spectra were obtained in the range 400~4000cm^{-1} with four scans at a resolution of 4 cm^{-1}.

2.3.2 The characterization of grafted product and CPE

ATR-FTIR spectroscopy.

ATR-FTIR analysis was carried out using a Perkin-Elmer Spectrum 100 in the wavenumber range of 4000 to 650 cm^{-1} at room temperature.

Differential scanning calorimetry (DSC)

Grafted products of ENR-*g*-mPEG-COOH were tested by DSC, TA Q2000 instrument (TA instrument, USA). ENR-*g*-mPEG-COOH matrix were sealed in hermetic aluminum pans and scanned at a heating of 20 °C·min^{-1} under a nitrogen flow. In each case, the following cycle was used: cooling at a rate of 20 °C min^{-1} from room temperature to -50°C, heating at a rate of 20 °C min^{-1} to 120°C, cooling at 10°C min^{-1} to -50°C and heating at the same rate of 20 °C·min^{-1} up to 100°C.

The ENR-*g*-mPEG-COOH/$LiClO_4$ CPE are tested in the same method.

The equilibrium swelling method

The crosslink density of the ENR-*g*-mPEG-COOH/$LiClO_4$ CPE was determined by the equilibrium swelling method[21]. The samples were first weighed to calculate their initial dry weight (m_1), then they were inserted into bottles containing 50 mL toluene at 23°C for three days until swelling equilibrium. Solvent on the surfaces of the samples were removed, then samples were weighed to determine their equilibrium weight (m_2). The samples then were dried in an oven under 60°C for 24 hours and reweighed to determine the final dry weight (m_3). The crosslinking density was calculated from the Flory-Rehner equation:[22]

$$\nu_e = -\frac{1}{v}\left[\frac{\ln(1-\nu_2)+\nu_2+\chi\nu_2^2}{\nu_2^{1/3}}\right] \quad (1)$$

In Eq. 1, ν_e is the crosslink density (in mole per unit volume), v is the molar volume of the solvent, ν_2 is the volume fraction of the polymer in the swollen mass and calculated according to Eq. 2, and χ is the Flory-Huggins polymer-solvent interaction parameter calculated with Eq. 3,

$$\nu_2 = \frac{m_3/\rho}{\frac{m_3}{\rho}+\frac{m_2-m_1}{\rho_s}} \quad (2)$$

$$\chi = \frac{v}{RT}(\delta_1 - \delta_2)^2 \quad (3)$$

where ρ is the density of the polymer, ρ_s is the density of the solvent, R is the gas constant and T is the absolute temperature, δ_1 is the solubility parameter of solvent and δ_2 is the solubility parameter of polymer.

XRD measurements

XRD measurements were carried out at room temperature on a D/MAX-2200/PC diffractometer (Rigaku Co. Ltd., Japan), using the Cu Kα radiation at 40 kV/40 mA for 2θ values between 5°and 60° with a scanning speed of 6 °/min.

Ionic conductivity

Ionic conductivity was measured by alternating current complex impedance analysis using Auto-lab PGSTA302 electrochemical test system at room temperature. The frequency ranged from 1 MHz to 1 Hz and the signal amplitude was 10 mV. The polymer solid electrolyte was sandwiched between the stainless steel ion-blocking

electrodes with a surface contact area of 1 cm^2. The conductivity (σ) can be calculated from the Eq. 4 [23-25],

$$\sigma = \frac{d}{R_b S} \qquad (4)$$

where d is the sample thickness, S is the active area of the electrode, R_b is the bulk resistance determined from the equivalent circuit analysis.

3. Results and Discussion

3.1 *In situ* FTIR spectroscopy

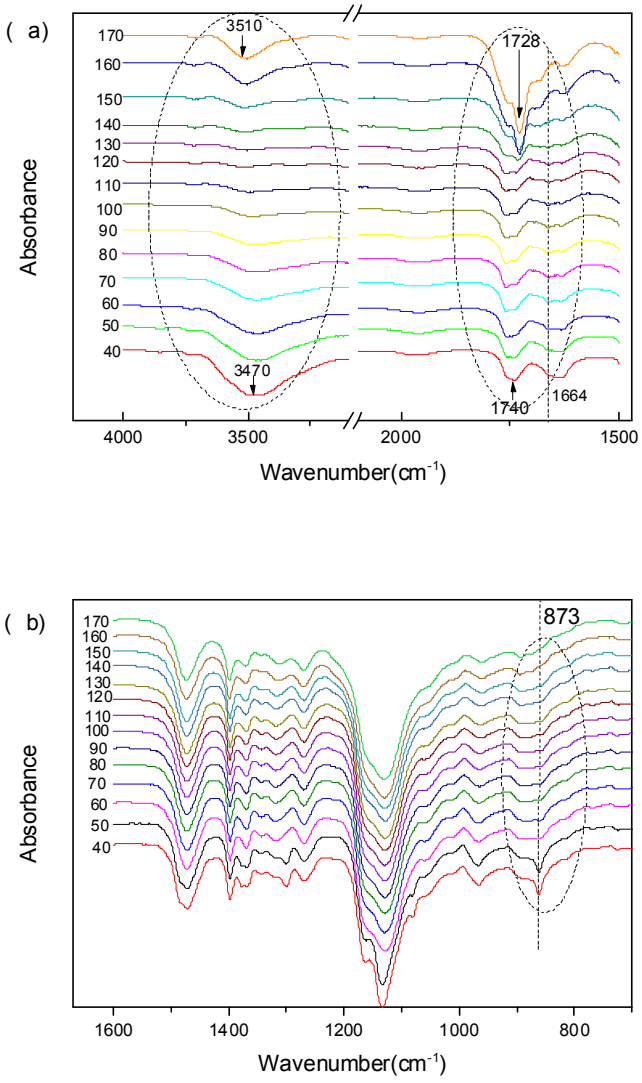

Fig. 2 *In situ* FTIR spectra of ENR 50/mPEG-COOH compound (40~170°C): (a) 4000~1500 cm^{-1} (b) 1600~800cm^{-1}

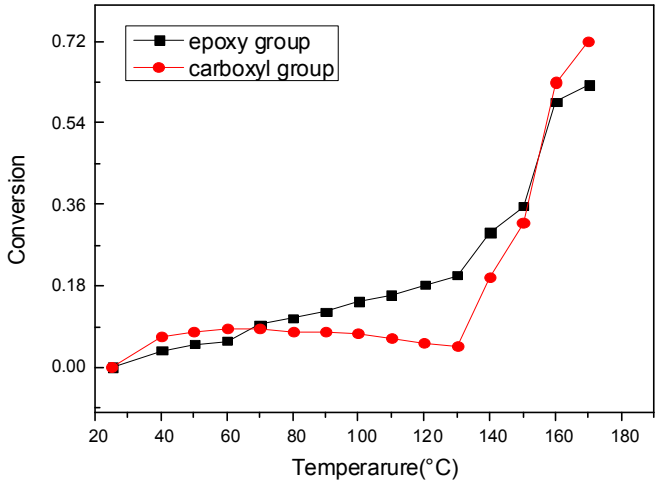

Fig. 3 Conversion of epoxy and carboxyl groups on different temperature

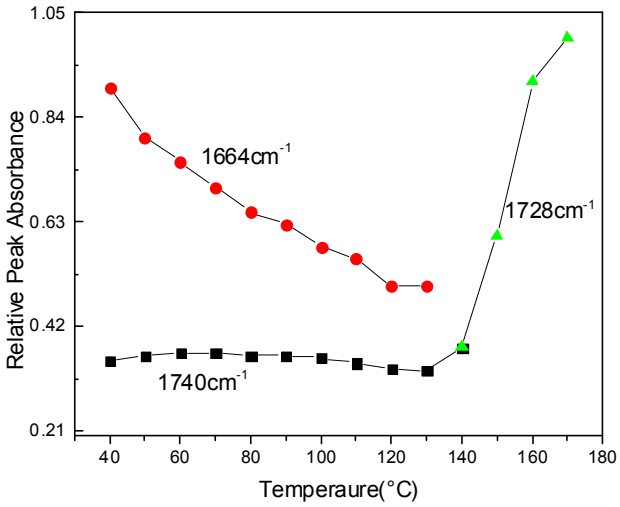

(a) C=O stretch

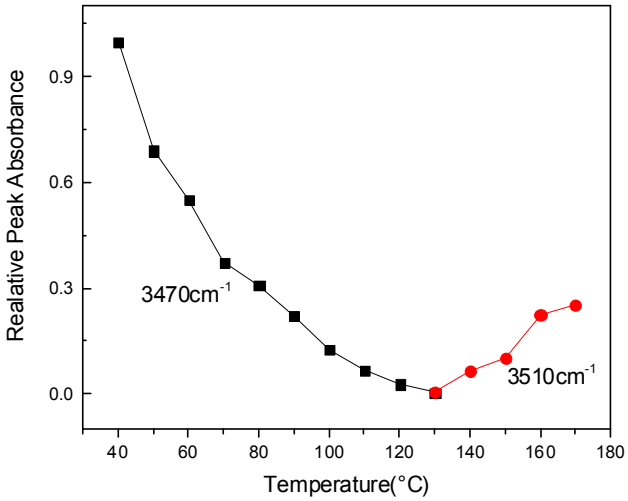

(b) O-H stretch

Fig. 4 Temperature dependence of relative peak absorbance: (a) C=O stretch (b) O-H stretch

In situ FTIR spectra of ENR/mPEG-COOH (100/80) compound is shown in Fig. 2. ENR 50 has the same absorption peaks with the basic characteristics of natural rubber, such as C-H stretching mode at 2960 and 2920 cm^{-1}, [26, 27] C=C stretching mode at 1651 cm^{-1} and CH_2 scissoring mode at 1451 cm^{-1}.[28] The characteristic absorption peak of ENR 50 is the C-O-C stretching mode of epoxy ring at 873 cm^{-1}. Using the absorption peak at 873 cm^{-1} to evaluate the content of epoxy groups is well documented[29, 30]. The characteristic absorption peaks corresponding to the carboxyl group of mPEG-COOH at 1740 and 948 cm^{-1} are attributed to the free carboxyl C=O and C-O stretching vibrations, respectively. Peaks at 873 cm^{-1} (epoxy groups in ENR 50) and 1740 cm^{-1} (C=O stretch of carboxyl groups in mPEG-COOH) gradually disappear, new peaks at 3510 cm^{-1} (stretching vibrations of O-H hydroxyl groups) and 1728 cm^{-1} (C=O of ester bonds) are observed with increasing temperature. This implies that ENR 50 has reacted with mPEG-COOH to form ENR-*g*-mPEG-COOH.

The process of grafting reaction of ENR 50 and mPEG-COOH was investigated by the intensity changes of absorption peaks at 873, 1740, 1728 and 3470 cm^{-1}. As the samples are unchanged during the reaction, the conversion of the epoxy group and the carboxyl group could be directly characterized by the area of these absorption peaks. The conversion was calculated based on Lambert-Beer law which is shown as

equation (5).

$$\alpha = \frac{(A_X^0/A_0^0)-(A_X^T/A_0^T)}{A_X^0/A_0^0} \quad (5)$$

According to actual situation, the formula was converted to

$$\alpha = \frac{A_X^0-A_X^T}{A_X^0} \quad (6)$$

where A_X^0 is the initial absorbance when the temperature is 25℃ at *x*=873 or 1740 cm^{-1}, or the maximum absorbance at the end of the process when the temperature is 170 ℃. A_X^T is the absorbance at temperature *T* at *x*=873 or 1740 cm^{-1}.

As shown in Fig. 3, the conversion of epoxy group and carboxyl group increased significantly with temperature increasing from 130℃ to 170℃, indicating the grafting reaction took place between epoxy and carboxyl groups.

Fig. 4. (a) and (b) show the relative intensity of the carbonyl C=O and hydroxyl O-H absorption peak at different temperatures, which are determined by the changes of their peak areas. Fig. 4(a) shows that the absorption peak intensity of the free carboxyl groups (1740 cm^{-1}) gradually decreases with increasing temperature. The hydrogen bonded carbonyl absorption peak intensity (1664 cm^{-1}) declines linearly with the increment of temperature until the absorption peak disappears at 140℃, and the peak position shifts to 1728 cm^{-1} which is corresponding to ester carbonyl group. The absorption intensity (1728 cm^{-1}) increases rapidly, which indicates that carboxyl group participate in the reaction to generate ester bond. As shown in Fig. 4(b), with the increment of temperature, the peak intensity of hydrogen bond gradually decreases at 140℃, meanwhile, free hydroxyl groups at 3510 cm^{-1} begins to appear. In addition, the intensity of the absorption peak of the alcohol hydroxyl (3510 cm^{-1}) increases as temperature increases. It is evident that consumption of carboxyl groups (3470 and 1740 cm^{-1}) is accompanied by the formation of hydroxyl groups (3510 cm^{-1}) and C=O groups of ester bonds (1728 cm^{-1}), which further confirms that the reaction between epoxy groups and carboxyl groups takes place during grafting.

3.2 Characterization of graft polymer ENR-*g*-mPEG

3.2.1 ATR-FTIR Spectroscopy

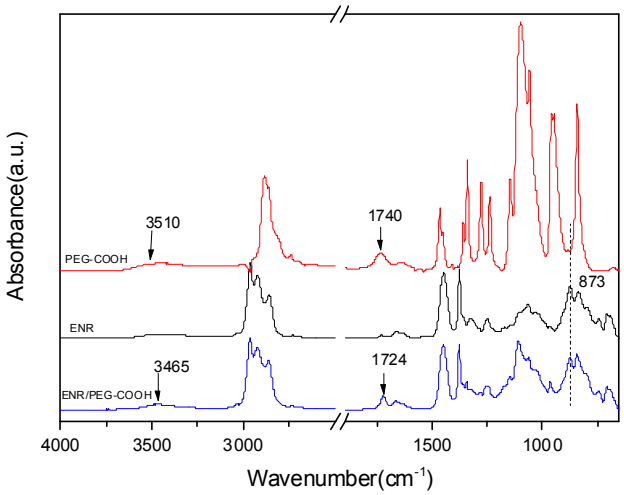

Fig. 5 ATR-FTIR spectra of purified ENR 50, pure mPEG-COOH and ENR-*g*-mPEG-COOH reaction products

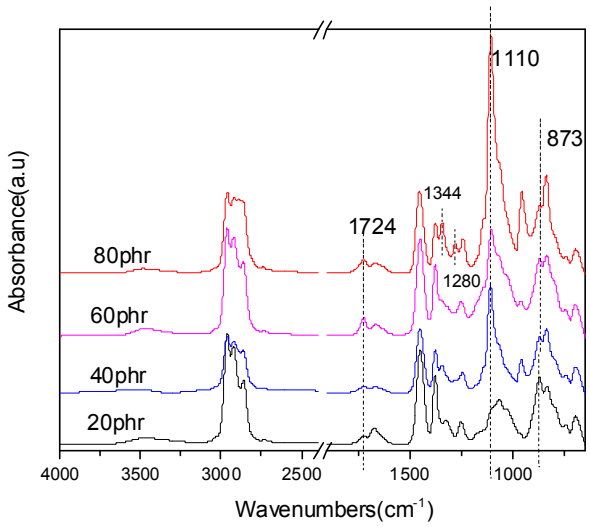

Fig. 6 ATR-FTIR spectra of ENR 50 grafted with varying content of mPEG-COOH after extraction

The grafting reaction of ENR 50 with mPEG-COOH can also be confirmed by the ATR-FTIR spectra as shown in Fig. 5. When ENR 50 and mPEG-COOH are mixed, reacted and extraction processed, the feature peak of carboxyl group in mPEG-COOH almost disappears and epoxy group in ENR 50 decreases. Meanwhile, the absorption bands of grafting polymer are observed around 3465 and 1724 cm^{-1}, which are corresponding to hydroxyl groups (-OH) and ester bonds (C=O), respectively. Fig. 6

shows the ATR-FTIR spectra of ENR 50 grafted with varying content of mPEG-COOH. The absorption peak of epoxy ring mode at 873 cm^{-1} decreases with increasing of mPEG-COOH content. The absorption peaks at 1724 cm^{-1} and 1110 cm^{-1} also increase, which respectively correspond to ester bond and ether bond. And there are two different peaks in CPE (80phr) from others: 1280 and 1344cm^{-1}. Peak at 1344cm^{-1} is attributed to a blend of ring δ_{CH} and of δ_{OCH} and δ_{CCH} in *trans*-OCH_2CH_2O. This indicating the gauche-OCH2CH2O- segments presumably in amorphous state. The emergence of new peak reveals that some (smaller) fraction of the C=O ester group has become bonded in a different environment[31]. The new bands at 1280cm^{-1} correspond to the C-O stretching vibration[32]. We can see the same peaks in spectra of mPEG-COOH in Fig 5. The peak of 1280cm^{-1} is different from others. I think that might be no complete reaction to mPEG-COOH and some residues in the mixture.

FT-IR spectroscopic analysis results demonstrate that more carboxyl group react with epoxy group with increasing of mPEG-COOH. The grafting reaction mechanism is shown in Scheme 1.

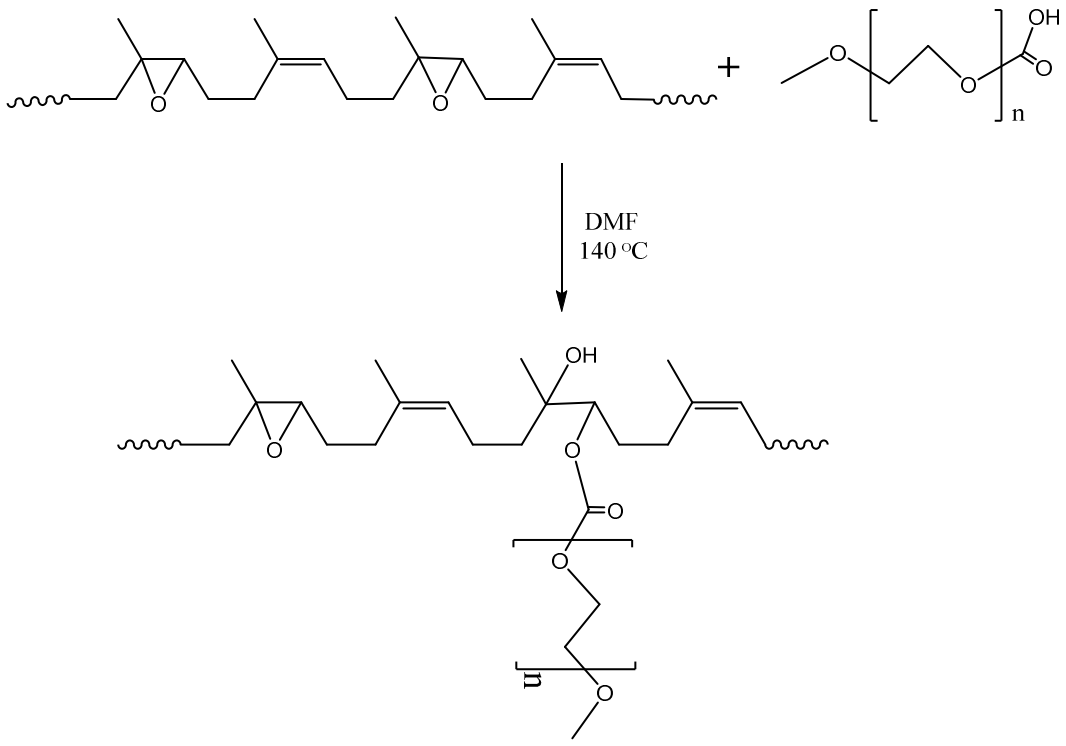

Scheme 1 Reaction mechanism of ENR 50 with mPEG-COOH

3.2.2 DSC analysis

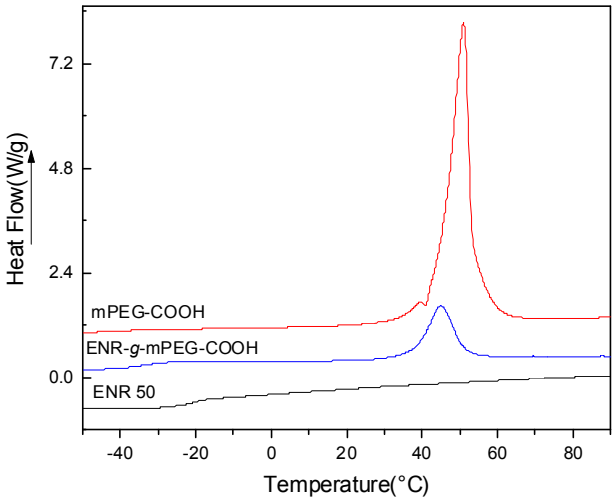

Fig.7 DSC curves of ENR 50, mPEG-COOH, ENR-*g*-mPEG-COOH

Table 1 Thermal analysis data from DSC curves

Samples	T_g (°C)	T_m (°C)	ΔH_m (J/g)	X_c (%)
ENR 50	-21.0	-	-	-
ENR-*g*-mPEG (100/80)	-31.1	44.8	32.8	15.3
mPEG-COOH	-	51.0	146.4	68.5

The crystallinity of the samples is relative to the quality of the mPEG-COOH after normalizing the processed data.

Fig. 7 shows the DSC curves of reactants and grafting products after extraction. Table 1 presents a summary of the main data from the curves. The relative crystallinity (X_c) could be calculated from the Eq. 7.

$$Xc=\frac{\Delta H_m^{sample}}{\Delta H_m^*}\times 100\% \quad (\Delta H_m^*=213.7 \text{ J/g}) \qquad (7)$$

In which ΔH_m^* is the melting enthalpy of a completely crystalline mPEG-COOH sample [33]. As shown in Fig. 7, the grafting of mPEG-COOH to ENR 50 causes the decreasing of T_g by 10°C, indicating a greater fraction of -OCH_2CH_2O- units contributes to a lower T_g. Compared with mPEG-COOH, the melting peak of ENR-*g*-mPEG-COOH shifts to lower temperature. Meanwhile, the crystallinity of

ENR-*g*-mPEG-COOH decreases from 68.5% to 15.3%, which indicates the crystallization of mPEG-COOH is inhibited and the crystalline size decreases when mPEG-COOH is grafted to ENR 50. The polymer chain segment moves more easily due to the introduction of mPEG and the increment of amorphous region. One of the main reasons is that the introduction of flexible side chains leads to an increment of the free volume of the polymer chains. The reduction of crystallinity and the decrement of T_g are beneficial to improve the ionic conductivity of CPE.

3.3 The characterization of ENR-*g*-mPEG-COOH/$LiClO_4$ CPE

3.3.1 DSC analysis

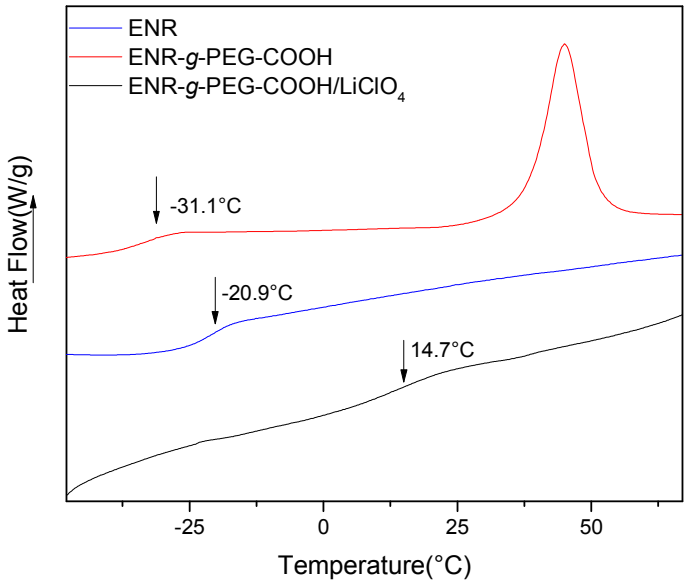

Fig.8 DSC thermographs of pure ENR 50, ENR-*g*-mPEG-COOH and ENR-*g*-mPEG-COOH/$LiClO_4$ CPE

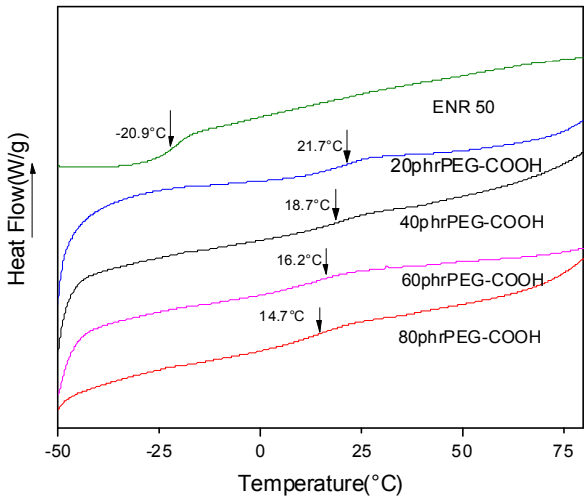

Fig.9 DSC thermographs of pure ENR 50, and ENR-*g*-mPEG-COOH/$LiClO_4$ CPE with various content of mPEG-COOH

Table 2 The T_g of CPE with varying mPEG-COOH

mPEG-COOH (phr)	T_g (°C)
0	-20.9
20	21.7
40	18.7
60	16.3
80	14.7

Fig. 8 shows the comparison of between ENR, ENR-*g*-mPEG and ENR-*g*-mPEG-COOH/$LiClO_4$ CPE. Compare with ENR-*g*-mPEG-COOH, the T_g of ENR-*g*-PEG-COOH/$LiClO_4$ CPE increase 35.6°C due to the addition of the lithium salt. The melting peak disappears in the curve of GPE with $LiClO_4$. The dissociation complexation interaction between Li^+ and $–OCH_2\text{-}CH_2O\text{-}$ units contribute to such variation.[12] Fig. 9 shows the DSC curves of pure ENR 50, and ENR-*g*-mPEG-COOH/$LiClO_4$ CPE with different mPEG-COOH contents. The T_g values of CPE are calculated from Fig. 9 and the results are shown in Table 2. Compared with pure ENR 50 and ENR-*g*-mPEG-COOH composites, the T_g of CPE increases significantly because of the addition of the lithium salt. The cause may be the complexation between Li^+ and the oxygen atom of oxirane group.[34] However, with increasing mPEG-COOH content, the T_g values of CPE reduce. Owing to a large

number of flexible groups on the mPEG-COOH, the mPEG-COOH may serve as the plasticizer[35].

3.3.2 Crosslink density

The swelling rate was estimated as

$$S_W = \frac{W_g - W_0}{W_0}, \quad (8)$$

where W_0 is the weight of the dry sample, and W_g is the weight of the swollen sample.

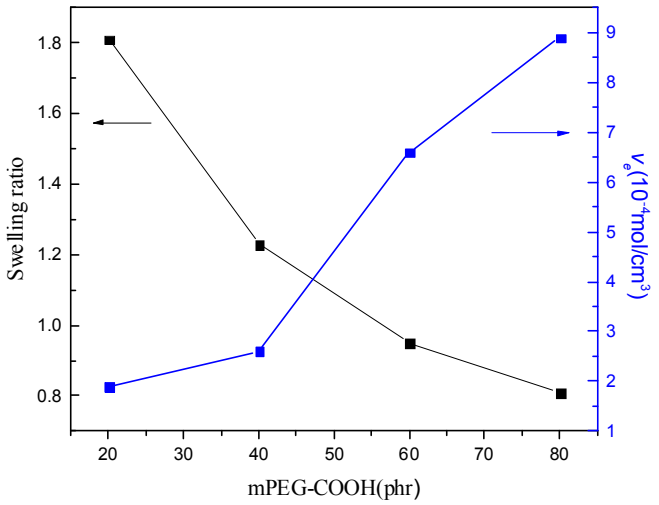

Fig. 10 Swelling ratio and crosslink density of ENR 50/mPEG-COOH/$LiClO_4$ composites polymer electrolyte

The swelling ratio and crosslink density of ENR-*g*-mPEG-COOH/$LiClO_4$ CPE are shown in Fig. 10. The lithium salt $LiClO_4$ was added into ENR-*g*-mPEG-COOH to introduce a crosslinking reaction to CPE. Lithium ion and polymer produced coordination crosslinking to make composite polymer swell without dissolving. With the increase of mPEG-COOH content, the swelling ratio decreases and crosslink density increases. The results indicate that the crosslink density of CPE increase with the increment of mPEG-COOH contents. The Li^+ coordinate with more oxygen atoms so that the crosslinking network is improved and the swelling ratio of CPE decreased

3.3.3 XRD analysis

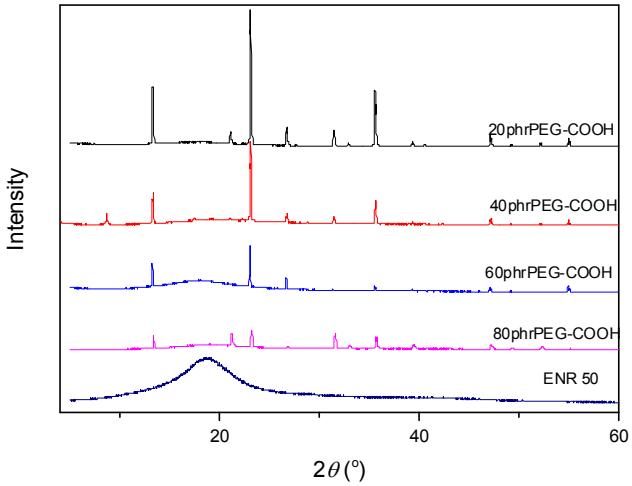

Fig.11 XRD spectra of ENR 50 and ENR-*g*-mPEG-COOH/$LiClO_4$ CPE with different mPEG-COOH content

Fig. 11 shows the XRD patterns of the ENR 50 and CPE samples with 40phr $LiClO_4$ and varied content mPEG-COOH from 20phr to 80phr. For pure ENR 50, no sharp peak appeared except for a single broad peak that suggested that ENR 50 is a fully amorphous polymer. The diffuse peak at 2θ of 20° is ascribed to ENR 50 while diffraction peaks at 2θ of 21.0°, 23.0° and 31.3° are ascribed to $LiClO_4$ crystals.[36] For ENR-*g*-mPEG-COOH/$LiClO_4$ composites, the sharp and tense diffraction peaks of $LiClO_4$ crystals indicate high crystallinity of $LiClO_4$ in the composite. With increasing mPEG-COOH content, the intensity of the diffraction peaks decreases gradually, which indicates the reduction of $LiClO_4$ crystals. This is caused by the interaction between $LiClO_4$ and mPEG-COOH, which contributes to the dissolution of $LiClO_4$ crystals. ENR 50 with strong polar epoxy groups can also dissolve lithium salt partly. The crystal solvation further increases so that more free Li^+ ions can be released, which is beneficial to the improvement of ionic conductivity of the CPE composites.

3.4 Ionic conductivity

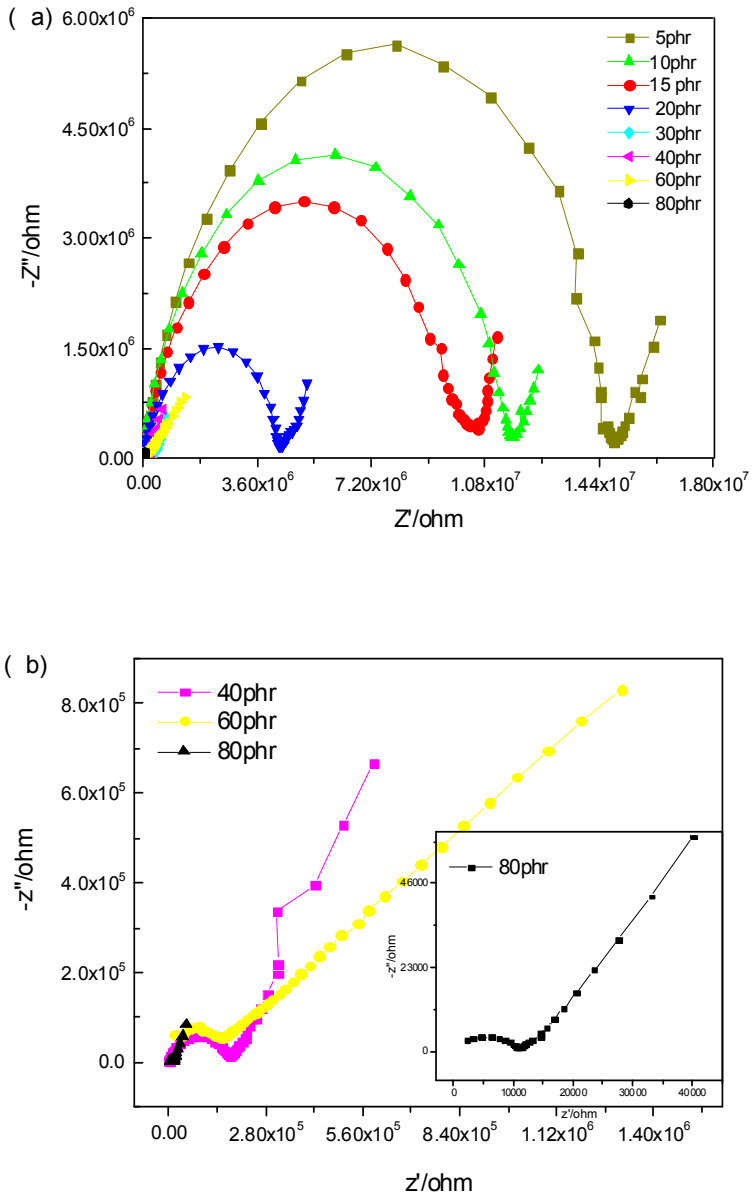

Fig.12 A.C. impedance spectra of the ENR-*g*- mPEG-COOH/ $LiClO_4$ solid electrolyte composites with different mPEG-COOH content: (a) from 5 phr to 80 phr, (b)40 phr to 80 phr

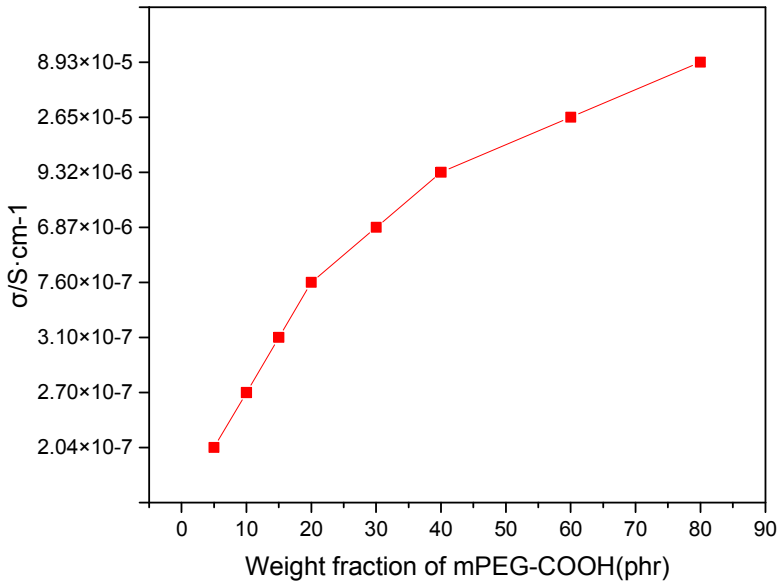

Fig.13 The ionic conductivity of the ENR-*g*- mPEG-COOH /$LiClO_4$ CPE

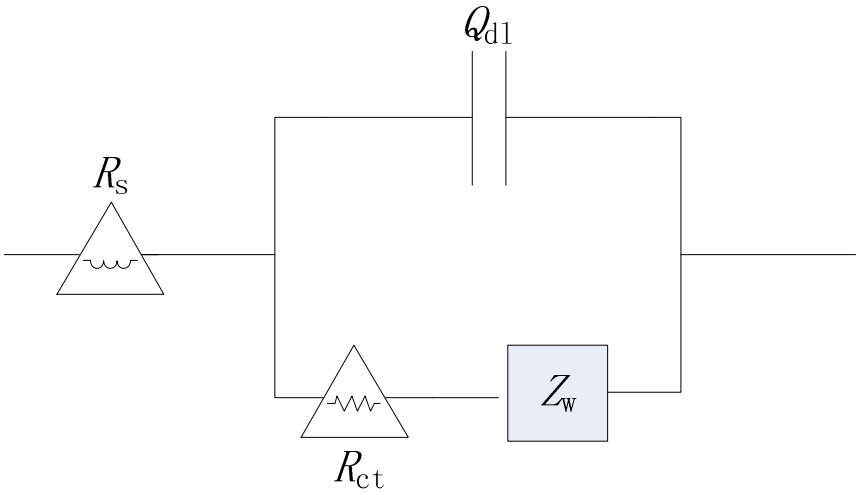

Fig. 14 Equivalent circuit used for fitting the impedance spectra of CPE thin film electrode.

Fig. 12 shows the impedance spectra of the ENR-*g*-mPEG-COOH/$LiClO_4$ CPE at 25°C as a function of mPEG-COOH content. The composition dependence of the CPE ionic conductivity is presented in Fig. 13 for better interpretation. The conductivity of CPE increases as the weight fraction of mPEG-COOH increases partly due to an increment of free Li^+ carrier quantity and decrement of polymer chain

entanglement within the test range. When the weight ratio of mPEG-COOH to ENR 50 is 0.8:1, the ionic conductivity reaches the maximum of 8.93×10^{-5} S·cm^{-1}. This is because the graft reaction between mPEG-COOH and ENR brings flexible chain segments to the polymer matrix, thus improves the interaction ability with lithium salt. The directional movement of Li^+ is achieved in the electric field. With the increments of mPEG-COOH contents, the conductivity of ENR-*g*-mPEG-COOH/$LiClO_4$ CPE will increase.

The simplified equivalent circuit model was constructed to analyze the impedance spectra in Fig. 14. The circuit comprise of The *R*s illustrates the resistive movement of charge carriers in CPE. R_{ct} and the constant phase element (Q_{dl}) are assigned to the charge transfer resistance and to the double layer capacitance, respectively. Z_w is the diffusion Warburg impedance. The element of Q_{dl}, R_{ct}, and Z_w arises from the double layer at the electrolyte interface in the system. The capacitive character of the double layer at the is denoted by a constant phase element instead of an ideal capacitor. In the impedance spectra, the high-frequency semicircle represents the Li^+ embedded firstly transfer-across the activity SEI films of the electrode surface; the low frequency line represents the active Li^+ diffuse in the electrode. According to the equivalent circuit and the impedance spectra, the CPEs follow a common conduction mechanism. In CPE, two process may occur in the interface region, the charge carries, typically Li^+ ions hop along the polar site. They transfer across the interface itself and formation of double layers due to the development of potential drop at electrode surface, which would introduce Li^+ concentration gradients in the electrolyte. The Li^+ would be driven to move in bulk electrode or out into the electrolyte by the concentration gradients.[1, 3, 37]

4. Conclusions

ENR-*g*-mPEG-COOH graft polymer was successfully prepared *via* a graft reaction between ENR 50 and mPEG-COOH. The process of grafting reaction was investigated by *in situ* FTIR. FTIR result indicates that the carboxyl group of mPEG-COOH can react with the epoxy group of ENR 50 to generate the

ENR-*g*-mPEG-COOH composites. DSC analysis shows that the melting temperature, the enthalpy of fusion, and the normalized crystallinity of grafted product were significantly lower than that of mPEG-COOH. In addition, ENR-*g*-mPEG-COOH/$LiClO_4$ composites electrolyte were prepared through introducing $LiClO_4$ into the ENR-*g*-mPEG-COOH graft system and the CPE was studied by DSC, the equilibrium swelling method and XRD. The increment of T_g and the analysis of crosslink density can also prove the formation of Li^+ and polymer coordination crosslinking. The ionic conductivity of CPE increases with raising mPEG-COOH content. The ionic conductivity reaches the maximum of 8.93×10^{-5} $S\cdot cm^{-1}$. And the mechanism of Li^+ transportation in the CPE is explained by the equivalent circuit.

Acknowledgements

The authors would like to extend their sincere appreciation to the National Nature Science Foundation of China (Grant No. 51373095)

Notes and references

1. W. L. Tan and M. Abu Bakar, *Ionics*, 2016, **22**, 1319-1335.
2. C. H. Chan, H.-W. Kammer, L. H. Sim, S. N. H. M. Yusoff, A. Hashifudin and T. Winie, *Ionics*, 2014, **20**, 189-199.
3. W. L. Tan, M. Abu Bakar and N. H. H. Abu Bakar, *Ionics*, 2013, **19**, 601-613.
4. T. K. Lee, A. Ahmad, Y. Farina, H. M. Dahlan and M. Y. A. Rahman, *Journal of Applied*

Polymer Science, 2012, **126**, E159-E165.

5. B. Sun, P. Tehrani, N. D. Robinson and D. Brandell, *Journal of Materials Science*, 2013, **48**, 5756-5767.
6. S. Guinot, E. Salmon, J. Penneau and J. Fauvarque, *Electrochimica Acta*, 1998, **43**, 1163-1170.
7. L. Y. Yang, D. X. Wei, M. Xu, Y. F. Yao and Q. Chen, *Angewandte Chemie International Edition*, 2014, **53**, 3631-3635.
8. N. Boden, S. Leng and I. Ward, *Solid State Ionics*, 1991, **45**, 261-270.
9. M. Marzantowicz, J. Dygas, F. Krok, A. Łasińska, Z. Florjańczyk, E. Zygadło-Monikowska and A. Affek, *Electrochimica acta*, 2005, **50**, 3969-3977.
10. L. TianKhoon, N. Ataollahi, N. H. Hassan and A. Ahmad, *Journal of Solid State Electrochemistry*, 2016, **20**, 203-213.
11. Q. Lin, *British Journal of Pharmacology*, 2015, **5**, 437-444.
12. M. Li, W. Ren, Y. Zhang and Y. Zhang, *Journal of Polymer Research*, 2012, **19**, 1-7.
13. Y. Lu, Q. Lin, W. Ren and Y. Zhang, *Journal of Polymer Research*, 2015, **22**, 1-10.
14. Z. Zhu, M. Hong, D. Guo, J. Shi, Z. Tao and J. Chen, *Journal of the American Chemical Society*, 2014, **136**, 16461-16464.
15. F. Latif, M. Aziz, A. M. M. Ali and M. Z. A. Yahya, *Macromolecular Symposia*, 2009, **277**, 62-68.
16. R. Idris, M. D. Glasse, R. J. Latham, R. G. Linford and W. S. Schlindwein, *Journal of Power Sources*, 2001, **94**, 206-211.
17. M. L. Hallensleben, S. H. Rüdiger and R. H. Schuster, *Journal of Histochemistry & Cytochemistry Official Journal of the Histochemistry Society*, 1995, **227**, 643-652.
18. F. Harun and C. H. Chan, in *Flexible and Stretchable Electronic Composites*, eds. D. Ponnamma, K. K. Sadasivuni, C. Wan, S. Thomas and M. Al-Ali AlMa'adeed, Springer International Publishing, Cham, 2016, DOI: 10.1007/978-3-319-23663-6_2, pp. 37-59.
19. W. Huang, Z. Zhu, L. Wang, S. Wang, H. Li, Z. Tao, J. Shi, L. Guan and J. Chen, *Angewandte Chemie International Edition*, 2013, **52**, 9162-9166.
20. E. Quartarone and P. Mustarelli, *Chemical Society Reviews*, 2011, **40**, 2525-2540.
21. J.-S. Chen, C. K. Ober, M. D. Poliks, Y. Zhang, U. Wiesner and C. Cohen, *Polymer*, 2004, **45**, 1939-1950.
22. P. J. Flory and J. Rehner, *The Journal of Chemical Physics*, 1943, **11**, 521-526.
23. L. J. Goujon, A. Khaldi, A. Maziz, C. Plesse, G. T. Nguyen, P.-H. Aubert, F. Vidal, C. Chevrot and D. Teyssié, *Macromolecules*, 2011, **44**, 9683-9691.
24. J. Luo, A. H. Jensen, N. R. Brooks, J. Sniekers, M. Knipper, D. Aili, Q. Li, B. Vanroy, M. Wubbenhorst, F. Yan, L. Van Meervelt, Z. Shao, J. Fang, Z.-H. Luo, D. E. De Vos, K. Binnemans and J. Fransaer, *Energy & Environmental Science*, 2015, **8**, 1276-1291.
25. X. Chen, H. Tang, T. Putzeys, J. Sniekers, M. Wubbenhorst, K. Binnemans, J. Fransaer, D. E. De Vos, Q. Li and J. Luo, *Journal of Materials Chemistry A*, 2016, **4**, 12241-12252.
26. E. Mertzel and J. L. Koenig, in *Epoxy Resins and Composites II*, Springer, 1986, pp. 73-112.
27. S. Noor, A. Ahmad, I. Talib and M. Rahman, *Ionics*, 2010, **16**, 161-170.
28. Q. Lin, Y. Lu, W. Ren and Y. Zhang, *RSC Advances*, 2015, **5**, 90031-90040.
29. H. Dannenberg and W. Harp Jr, *Analytical Chemistry*, 1956, **28**, 86-90.
30. N. Zainal, R. Idris and M. Nor Sabirin, 2011.

31. M. Urbanová, J. Šubrt, A. Galíková and J. Pola, *Polymer Degradation and Stability*, 2006, **91**, 2318-2323.
32. M. Laskoski, M. B. Schear, A. Neal, D. D. Dominguez, H. L. Ricks-Laskoski, J. Hervey and T. M. Keller, *Polymer*, 2015, **67**, 185-191.
33. X. Li and S. Hsu, *Journal of Polymer Science: Polymer Physics Edition*, 1984, **22**, 1331-1342.
34. S. N. H. M. Yusoff, S. L. Har, C. C. Han, A. Hashifudin and H.-W. Kammer, *Polymers Research Journal*, 2013, **7**, 159.
35. A. Ahmad, M. Y. b. A. Rahman and I. A. Talib, *Natural Science*, 2010, **2**, 190.
36. R. Baskaran, S. Selvasekarapandian, N. Kuwata, J. Kawamura and T. Hattori, *Solid State Ionics*, 2006, **177**, 2679-2682.
37. J. H. Lee and K. J. Kim, *Electrochimica Acta*, 2013, **102**, 196-201.